Computers & Geosciences 36 (2010) 921–935

Contents lists available at ScienceDirect

Computers & Geosciences

journal homepage: www.elsevier.com/locate/cageo

Using a composite grid approach in a complex coastal domain to estimate estuarine residence time

John C. Warner [a,*], W. Rockwell Geyer [b,1], Hernan G. Arango [c,2]

[a] U.S. Geological Survey, Coastal and Marine Geology Program, 384 Woods Hole Rd, Woods Hole, MA 02543, USA
[b] Woods Hole Oceanographic Institution, Applied Ocean Physics and Engineering, 98 Water Street, Mail Stop 12, Woods Hole, MA 02543, USA
[c] Institute of Marine and Coastal Sciences, Rutgers-The State University of New Jersey, 71 Dudley Road, New Brunswick, NJ 08901-8521, USA

ARTICLE INFO

Article history:
Received 26 June 2009
Received in revised form
21 October 2009
Accepted 23 November 2009

Keywords:
Residence time
Estuary
Three-dimensional model
Hudson river estuary
ROMS
Composite grid

ABSTRACT

We investigate the processes that influence residence time in a partially mixed estuary using a three-dimensional circulation model. The complex geometry of the study region is not optimal for a structured grid model and so we developed a new method of grid connectivity. This involves a novel approach that allows an unlimited number of individual grids to be combined in an efficient manner to produce a composite grid. We then implemented this new method into the numerical Regional Ocean Modeling System (ROMS) and developed a composite grid of the Hudson River estuary region to investigate the residence time of a passive tracer. Results show that the residence time is a strong function of the time of release (spring vs. neap tide), the along-channel location, and the initial vertical placement. During neap tides there is a maximum in residence time near the bottom of the estuary at the mid-salt intrusion length. During spring tides the residence time is primarily a function of along-channel location and does not exhibit a strong vertical variability. This model study of residence time illustrates the utility of the grid connectivity method for circulation and dispersion studies in regions of complex geometry.

Published by Elsevier Ltd.

1. Introduction

Residence time can be defined as a measure of retention within defined boundaries (Zimmerman, 1976). It is an estimate of time required for a particular substance to escape a region, and the residence time is extremely useful to determine water contamination and nutrient levels, distributions of organisms, and their spatio-temporal variations in bays and estuaries (Aikman and Lanerolle, 2004). Estimates also provide a measure of the timescale of physical exchange that can be compared with timescales of other processes, whether they are physical, chemical, or biological. In association with residence time is the concept of age, defined as the mean time elapsed since the particle under consideration entered into a region (Liu et al., 2008).

Estimation of residence time is difficult to quantify. Observational efforts are often hampered due to the limiting capability to measure introduced tracers into the system because they become spread out over a large region and the concentrations become too dilute to measure accurately. Previous numerical investigations have focused on several approaches. One approach is to release particles in a system (Wolanski, 2007) and measure the time for the particles to exit. Other approaches utilize the two distinctive concepts of age and residence time (Monson et al., 2002; Gourge et al., 2007). The age is defined as the time elapsed since the particle under consideration left a certain region (or entered a region) (Deleersnijder et al., 2001; Liu et al., 2008). The residence time is the complement of age, and is the time taken for the material to reach the outlet (Bolin and Rhode, 1973; Takeoka 1984; Yuan et al., 2007). The residence time is determined based on a remnant function to define the amount of material remaining in the water body and is computed as the time integral of the model-predicted concentration distribution over the model domain, divided by the initial amount of material in the water body. Other more advanced methods use an adjoint advection–diffusion method (Delhez et al. 2004; Zhang et al., 2010). In this study we choose to follow the method as described in Yuan et al., 2007 following Takeoka (1984) to compute the residence time as the integrated concentration from individual point source releases divided by the initial amount.

The residence time in an estuary is controlled mainly by the strength of the estuarine circulation and tidal dispersion processes. Interestingly, these processes tend to vary inversely with each other. As tidal amplitude increases, the mixing increases, and the strength of the estuarine exchange flow

* Corresponding author. Tel.: +1 508 457 2237; fax: +1 508 457 2310.
E-mail addresses: jcwarner@usgs.gov (J.C. Warner), rgeyer@whoi.edu (W. Rockwell Geyer), arango@marine.rutgers.edu (H.G. Arango).
[1] Tel.: +1 508 289 2868; fax: +1 508 457 2194.
[2] Tel.: +1 732 932 6555 × 266; fax: +1 732 932 6520.

0098-3004/$ - see front matter Published by Elsevier Ltd.
doi:10.1016/j.cageo.2009.11.008

decreases (Geyer and Cannon, 1982; Geyer et al., 2000), thus potentially increasing the residence time. Conversely, stronger tidal velocities cause greater horizontal dispersion which can decrease residence time (Zimmerman, 1986). So depending on the relative strength of these processes, estuarine exchange may increase or decrease with changes in tidal amplitude.

To investigate these processes of residence time we have selected the Hudson River. This estuary is a partially mixed system that has a pronounced spring-neap variation in stratification and circulation and this variation causes strong modulation of the salt transport (Bowen and Geyer, 2003; Lerczak et al., 2006). These variations would be expected to have a significant influence on residence time, although it is not obvious a priori whether residence time would increase during neap or spring tides. Additionally, the vertical and along-estuary placement of a tracer release may also dramatically affect the residence time, as the estuarine circulation can create different pathways for material transport through the system.

To investigate these processes numerically we utilize the Regional Ocean Modeling System (ROMS; Shchepetkin and McWilliams, 2005; Haidvogel et al., 2008). ROMS is a free-surface, hydrostatic model that solves the three-dimensional Reynolds-averaged form of the Navier–Stokes equations using finite-difference formulations on a horizontal curvilinear grid and vertical stretched terrain-following coordinates. The model contains high order advection schemes, a fourth-order accurate pressure gradient solver, a two-equation turbulence closure model, and is designed to perform efficiently on multiple processor computer systems.

This model has previously been shown to effectively reproduce the estuarine circulation and salt balance in the Hudson River Estuary system by Warner et al. (2005a). That application was limited to the estuarine and upstream, riverine region of the system and required the application of a dynamic boundary condition for the salinity at the southern end of the model domain. However, that boundary condition could not be generalized for other tracers. Therefore, to effectively investigate the system for residence time of a passive tracer, the model domain needed to be extended southward. This extension included a region of strongly variable coastline and connecting river systems. These types of configurations can be challenging for a structured grid numerical model. Previous efforts to study these types of regions would require extensive use of land masking or some type of grid deforming method. To overcome these difficulties we developed a new method that allows for multiple grids to be seamlessly connected, thus increasing the capability of a structured grid model for computing circulation and tidal processes in regions of strongly varying coastline. This method is similar to previous efforts such as by Eby and Holloway (1994) who developed a grid transformation to couple the Arctic to a larger scale ocean model and Dietrich et al. (2008) who developed a coupled multi-grid to investigate Mediterranean outflows using a method that exchanged fluxes across grid connections. Our method extends these previous formulations by using non-rotated connectivity and exchanging prognostic variables, thus yielding results that are not dependent on the location of the grid coupling.

The organization of this paper is as follows. Section 2 describes the method of developing the composite grid system for a structured grid model and provides a simple test case to demonstrate the functionality of the method. Section 3 describes the application of this new method to study the residence time of passive tracers in the Hudson River Estuary. Results are presented for releases at various locations and at different phases of the spring-neap cycle. Section 4 is summary and conclusions.

2. Methods

2.1. Existing methods to model strongly varying topography

Regions of strongly varying coastline pose a challenge for numerical models. One approach is to use unstructured grids that allow greater flexibility for discretizing complex domains. Grids developed with an unstructured mesh can more easily follow a coastline or more easily allow increased resolution in regions of localized flow phenomena. A disadvantage of unstructured grid models is that they typically use lower order (second-order accurate) advection schemes and then require increased resolution to obtain the same level of accuracy as structured grid models. This can lead to increased computational time, depending on the grid architecture. There are several reviews comparing structured and unstructured grids (for example Deleersnijder and Lermusiaux, 2008). Our intent is not to debate the issue but to provide insight and demonstrate an advancement of the structured grid approach.

A structured grid model can more easily employ higher order accurate advection schemes (third and fourth order) and the structured nature of the grid allows for a more efficient code. Disadvantages are that the structured grid has difficulties to provide increased resolution at localized regions in the grid. However, there are recent strong developments of grid refinement techniques (for example, Penven et al., 2006; Debreu and Blayo, 2008) and adaptive mesh refinement algorithms (Barad et al. 2009) that allow structured grids to have increased local resolution. Other approaches of structured grids to overcome difficulties to follow complex coastlines include grid curvature, masking, and stretching. Grid curvature is a method to align the grid to follow coastal or bathymetric features. The structured grid remains orthogonal and the method manipulates the grid design to allow concentrations of cells in an active region of interest. A drawback of grid curvature is that some parts of the domain may be curving in one direction but curving in a different direction elsewhere, making it difficult to manipulate the grid in a manner that follows the curvatures in all regions. A second method of grid manipulation is to use land/sea masking arrays. These arrays contain numerical values of 0 or 1 and are used during the computations to multiply prognostic values. The zero of the masked array will negate values computed on land cells. This method can still be very efficient in that the model loops are still vectorized over all rows and columns. Disadvantages of masking are that the method requires additional multiplicative factors included in the computation and poorly constructed grids may contain excessive masked regions that vastly reduce the computational efficiency of the simulation. The third method is stretching, which allows for increased resolution near a region of interest and decreased resolution elsewhere. A disadvantage is that grid stretching extends across the entire domain and may provide increased resolution in regions that are not required, once again being inefficient.

2.2. Composite grid approach

The approach is to first create multiple, individual grids of different regions, and then connect those individual grids together in a manner that is efficient and does not alter the results of the numerical solution. There are many aspects of such an approach that are specific to a particular model (i.e., structured grid vs. unstructured grid, placement of prognostic variables on the grid, etc.). For our development, we use a structured grid model that solves the equations on an Arakawa "C" grid (Arakawa and Lamb,

1977). We will focus on the development on this grid type; however, the concept could be applied to other modeling systems.

For a "C" grid the prognostic variables are located such that the u (x)-component of the velocity is centered on the east and west faces, the v (y)-component of the velocity is centered on the north and south faces. For a three-dimensional implementation the w (z)-component is centered on the top and bottom face, and the ρ point is located in the geometric center of each computational cell. This grid configuration allows the model equations to be solved in a flux formulation, i.e., the flux divergence along the faces equates to the change in the variable property at the center of the cell. Therefore no interpolation is required to perform the computations.

In plan view, these cells are arranged to form a rectangular array (Fig. 1, Grid 1 or Grid 2). For each grid, a critical aspect is how to provide information along the four lateral edges. This information is provided by two different methods: a boundary condition or in a grid overlap region as part of a composite grid. In either case, this is numerically accomplished through the solution of the continuity and momentum equations. For example, a third-order momentum advection scheme requires a stencil of three points. For a boundary condition, information will typically only

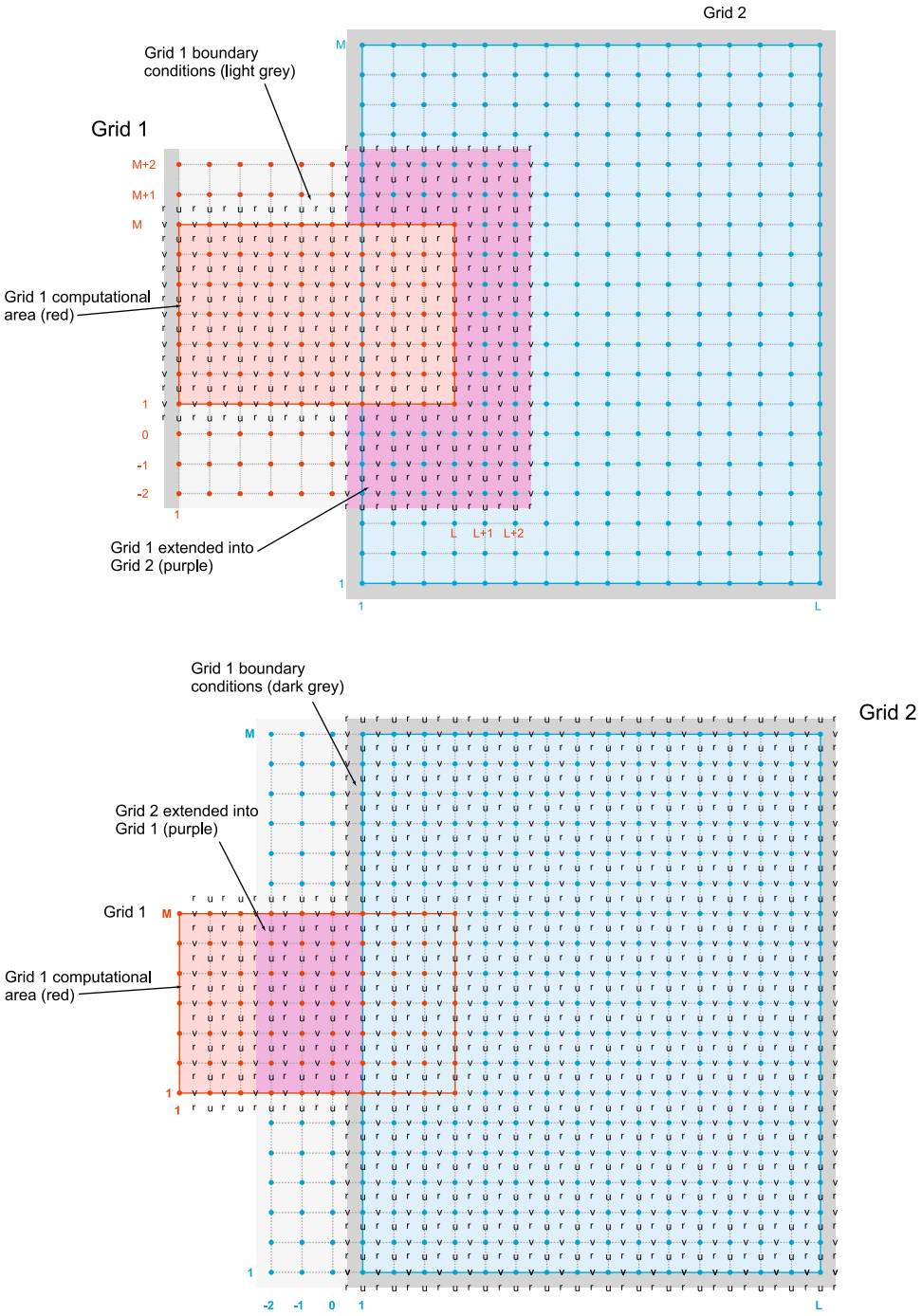

Fig. 1. Schematic of composed grids. Overlap regions are colored purple to identify extension of each grid into adjacent grid. (For interpretation of the references to color in this figure legend, the reader is referred to the web version of this article.)

be provided at one point and the model is making some type of assumption that may reduce the order (and hence the accuracy) of the advection scheme. However, for a composite grid using overlap regions, information is exchanged so that the model is provided with adequate information to allow the advection schemes to be solved over its full stencil. This methodology maintains the full original capability of the advection scheme. Issues of concern are determining what information is required in the overlap region, what information needs to be exchanged from/to another grid, and when to exchange it.

Our composite grid approach is as follows. Individual grids are developed separately for specific areas of the model domain. The individual grids are connected to adjacent grids in a very specific manner. This occurs with an overlap region. The overlap region is a section of the grid that overlaps an adjacent grid. For the current implementation, we restricted the overlap regions to be coincident—i.e., the grid cell sizes, orientation, and all properties are identical in the cells that overlap between grids. The rest of each grid can curve, have masking, and grid stretching in any manner. Only the overlap regions are coincident. If the approach is properly implemented, then the solution obtained by the composite grid formulation is identical to a solution obtained if there was only one large continuous grid. Therefore this method should not degrade the solution in any way.

The overlap regions are defined as shown in Fig. 1. Numerical models may have a variety of advection schemes and horizontal momentum mixing formulations that require different stencil footprints. The largest footprint in the x direction for the particular model we are using requires information at 4 u points to the left and 3 u points to the right of the interior computational area. The difference (4 left vs. 3 right) comes from the grid index numbering (i.e., a u point to the left of a ρ point will have the same index number). For Grid 1 (Fig. 1, top) the region colored light red is the interior computational region and extends from $i=1{:}L-1$ and $j=1{:}M-1$ for the ρ points. Lateral boundary conditions are required for the thick grey line along the western edge and includes one column of ρ and v points, and one column of u points. The light grey regions along part of the north and south edges also require boundary conditions, but for this example they are land-masked and do not require any information. The purple colored area is the grid overlap region. In this region Grid 1 requires information to be used by its advection schemes, mixing, etc. The purple area is larger than the typical boundary region of just 1 additional row or column of points because advection schemes typically require more than one data point. The purple overlap region requires Grid 1 to extend from $i=L{:}L+2$ and $j=-3{:}M+2$ (for ρ points). The data for these extra points are obtained from the next adjacent grid, i.e., Grid 2, or is land-masked (i.e., the light grey area).

Similarly, Grid 2 has an interior computational area (Fig. 1, bottom) that is colored light blue. The thick grey line along the northern, eastern, southern, and top and bottom parts of the western edges require external boundary conditions. The middle part of the western edge of Grid 2 requires lateral information. Grid 2 is extended into Grid 1 to provide an overlap region (purple area). This extension now requires Grid 2 to be larger in the western direction, but not larger in any other direction. The data for the purple overlap region are acquired from Grid 1.

Information at each grid point (in the interior region or the purple overlap regions) is only computed once, in either Grid 1 or Grid 2. The data are then exchanged to the other grid. This is accomplished in a delicate time stepping manner. This is described in a general manner as follows. As the model is time stepping, the main control loop calls specific subroutines in a well-defined order. For a non-composed grid application, the main time loop would just be executed in its entirety calling each subroutine in order for each time step. For a composed grid application, as the subroutines are called, they are executed for each grid in succession. This allows each grid to advance through the main time loop in a synchronous manner. The advantage of this time stepping method is that as each grid requires information in the purple overlap region, the adjacent grid that is providing that information is at the same time level and same sub-time step. This allows the data of the entire system to be solved in a synchronous fashion. The methodology is easily implemented because the model is based on an explicit time stepping.

There are several advantages to a composed grid approach. For example, for congruent grid spacing, the results will be identical no matter how the domain is combined or tiled. The approach allows for a natural extension of the advection schemes. There is no need to average fluxes. This method greatly reduces the masked regions and allows each grid to curve in its own direction. Disadvantages include the fact that each grid is now slightly larger (because of the overlap regions). The grids are also slightly more difficult to construct because the overlap regions are coincident. However, these disadvantages are outweighed by the advantage in computational efficiency gained by the composite grid approach.

2.3. "Dog-bone" test case

We implemented the composite grid approach as described in the last section into the ROMS (v. 3.0) model. As a simple example, we apply the composite grid method to study the gravity wave advection between two basins. The basins are connected via a narrow channel to yield a configuration that resembles a dog-bone (Fig. 2). Each basin is 2500 m long and 800 m wide, connected with a 200 m wide channel. The bathymetry is a constant 5 m deep. Values of zero land mask are located around the perimeter of the domain so that lateral boundary conditions are not required for this simple test. The initial conditions are zero velocity everywhere. A level free surface is initiated, except with an initial water surface displacement in the left basin that ramps from 1 m at the left wall to zero at $x=2000$ m. At onset, the sloping water surface establishes a freely propagating gravity wave to the right. The wave encounters the narrow channel and propagates through the channel to the right, entering the second bay. The wave reflects back from the walls and establishes an oscillation between the basins. The wave will continue until dissipated by bottom friction and internal viscous losses.

The approach is to solve the system in two ways. First the system is solved using a single continuous grid (Fig. 2A). This grid has cell sizes of 200 m in the x- and 20 m in the y-direction. The model is run with a time step of 5 s for a 5000 s simulation. Second, the system is solved with two grids connected as a composite grid system (Fig. 2B). Grid 1 and Grid 2 use the same time step and x- and y-cell sizes as the continuous grid. Both Grids 1 and 2 extend over the complete y-direction from $y=0$ to 1000 m. Grid 1 extends from $x=0$ to 5600 m, and Grid 2 extends from $x=4200$ to 10,000 m. This allows for an overlap region from $x=4200$ to 5600 m (i.e., both grids have cells that exist over this region). In the overlap region, Grid 1 solves the part of the grid that extends from $x=4200$ to 4800 m. Grid 2 solves for the region from $x=5000$ to 5600 m. During the time stepping, Grid 2 acquires the information from Grid 1 in the $x=4200$–4800 m range, and the Grid 1 acquires information from Grid 2 in the $x=5000$–5600 m range.

The solutions of the free surface and momentum of the continuous grid are identical to the composite grids solutions for all times in the simulation. The solution of the free surface at

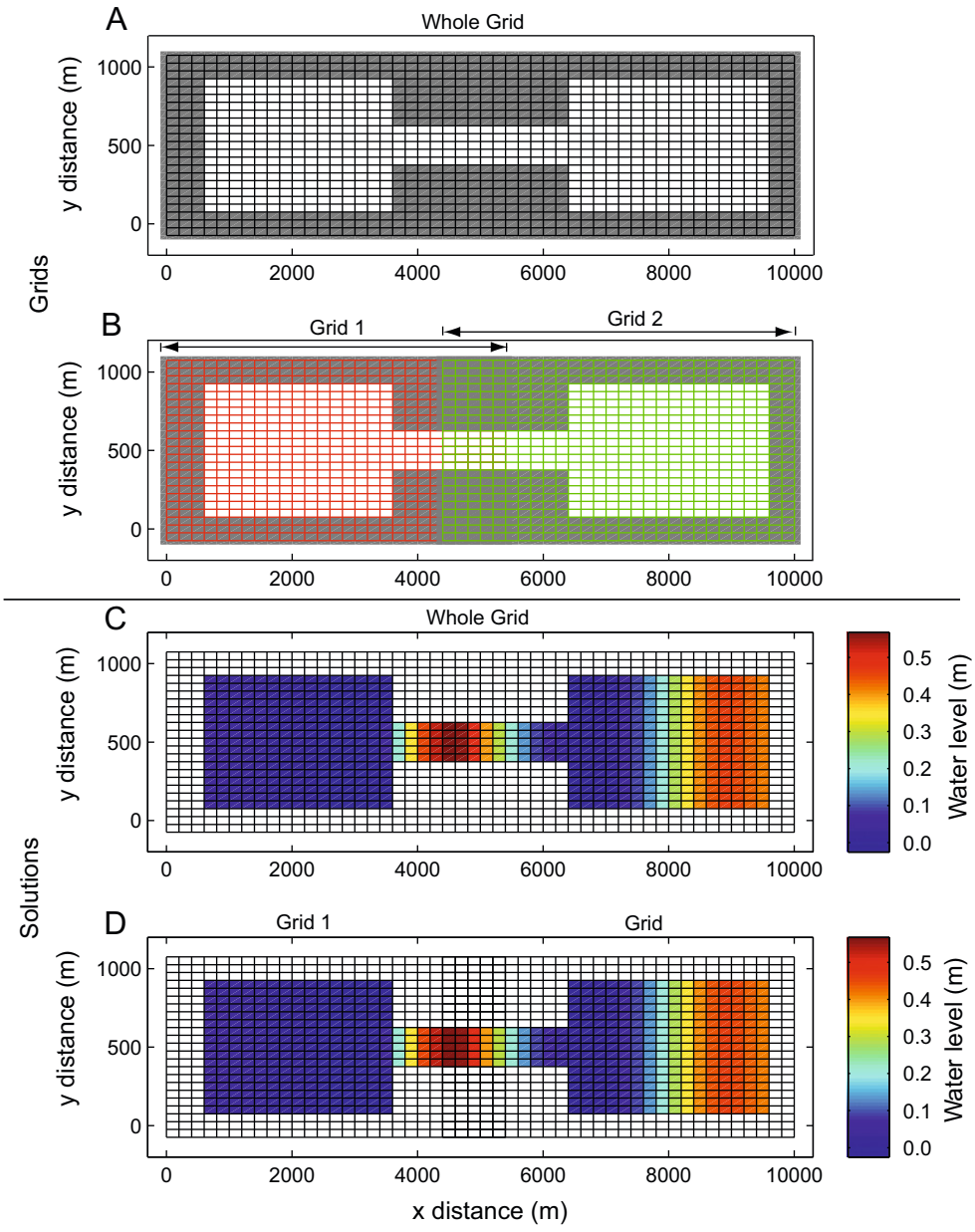

Fig. 2. Idealized 'dog-bone' test case to compare solution from a single continuous grid (panel A) to a composite configuration that uses two grids (panel B). Results of the simulations for the free surface are show for continuous grid (panel C) and for composite grids (panel D). Results are identical.

$t=4500$ s is shown in Fig. 2C and D for the continuous and the composed grids. The total computational times for both methods were equivalent. The purpose of this test is to demonstrate that our formulation is correct in that the composed grid does not introduce any numerical instabilities and yields identical results as compared to a continuous solution of the same region.

3. Hudson river residence-time calculation

The composite grid method was used to investigate the spatial and temporal transport and mixing processes in the Hudson River estuary. This application was selected because the results are particularly sensitive to the resolution of processes at the junction of the Hudson River, New York Harbor, and the East River. In the subsequent sections, first the grid configuration developed for the composite system is described. Then, the composed grid system is evaluated by comparing results of modeled salt transport to both observations and previous modeling efforts of salinity in the Hudson River estuary. The composite grid is then used to simulate a realistic dye release in the estuary and results are compared to observational data from a field study. Upon verification of the new composed grid modeling system, we then investigate the residence time of tracers released at different vertical and axial locations in the water column and at different phases of the spring/neap tide.

3.1. Composite grid for Hudson river system

Our main area of interest was the estuarine region of the Hudson River that extends from the Battery at the southern end of Manhattan northward for a distance of approximately 100 km. The Hudson River (Fig. 3) is located along the northeast coast of the United States. The tidal reach of the river extends from the Battery (at river km 0) to the Federal Dam at Troy, NY (at river km 250). The landward extent of salt in the estuary can reach to river

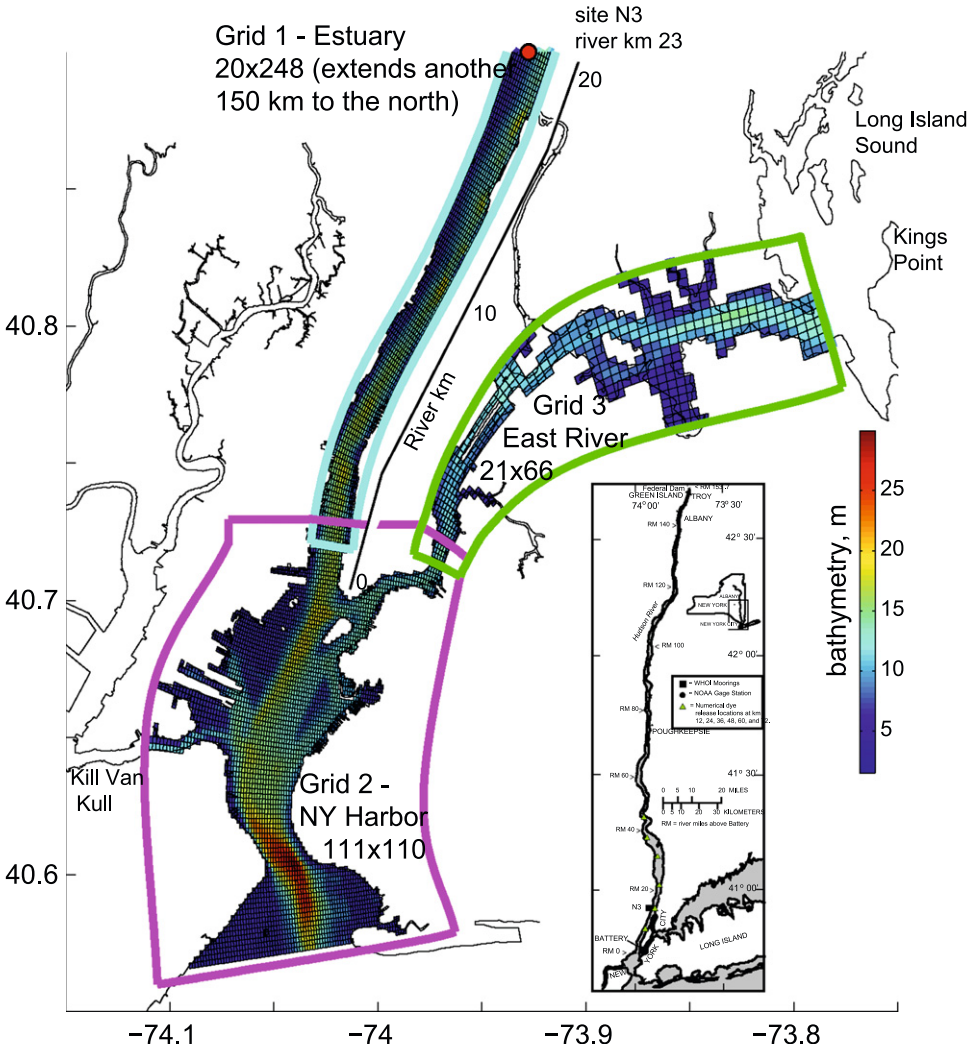

Fig. 3. Composed system showing connectivity of three independent grids for Hudson River application.

km 140 or as little as km 30 depending on freshwater discharge (Abood, 1974). The tidal range is of the order of 2 m and depth-mean tidal velocities reach 1 ms^{-1} during spring tides. Freshwater inflow has a mean summer (low flow) conditions approaching 200 $m^3 s^{-1}$ and maximum peak seasonal releases of the order of 2000 $m^3 s^{-1}$.

In a previous effort, Warner et al. (2005a) successfully developed and demonstrated the application of the ROMS model to simulate the salt flux and tidal processes in that region, using a domain that extended from the Battery northward to the dam near Albany. That effort utilized a natural northern boundary condition of a time-varying river discharge with known values of tracer quantities (i.e., salinity=0 and no passive tracers). For the southern boundary at the Battery we previously employed an empirically based condition for the salinity that depended on river discharge. However, to account for a passive tracer that would enter and leave the domain, a prescribed boundary condition would not be adequate, as there could be transient and variable storage of tracers within the Harbor. Therefore, instead of deriving a boundary condition for other tracers, it was determined that the model domain should be extended southward to include New York Harbor and the East River.

The New York Harbor is a major port and waterway. The harbor is approximately 20 km long and about 5 km wide. The harbor is dredged to maintain navigable channels. The East River is approximately 25 km long and connects the harbor to Long Island Sound. The river varies in width but narrows to approximately 300 m at its minimum width, creating strong tidal currents in this region that can exceed several meters per second.

For the application we developed a composite grid system composed of three grids (Fig. 3). Grid 1 for the Hudson River is similar to that from Warner et al. (2005a) and is a 20×248 mesh that extends from the Battery north to the Federal Dam. Grid spacing in the estuarine section is of the order of 100 m in the lateral direction and 250 m in the along-channel direction. The grid is linearly stretched in the along-channel direction with decreasing resolution in the northern riverine region. Grid 2 is for New York Harbor and is a 111×100 mesh with grid sizes of the order of 100 m in the lateral direction and 200 m in the along-channel direction. Grid 3 is for the East River and is comprised of 21 cells wide by 66 cells long. Near the connection to the harbor grid, the spacing of the East River grid is of the order of 200 m in the along-channel direction and increases to approximately 300 m near the northern end near the western end of Long Island Sound. All 3 grids are discretized in the vertical dimension with 20 terrain-following sigma levels and a vertical stretching parameter that was set to allow slight increase in resolution near the surface and bottom boundaries.

The surface, bottom, northern, and southern momentum boundary conditions were set to be consistent with Warner

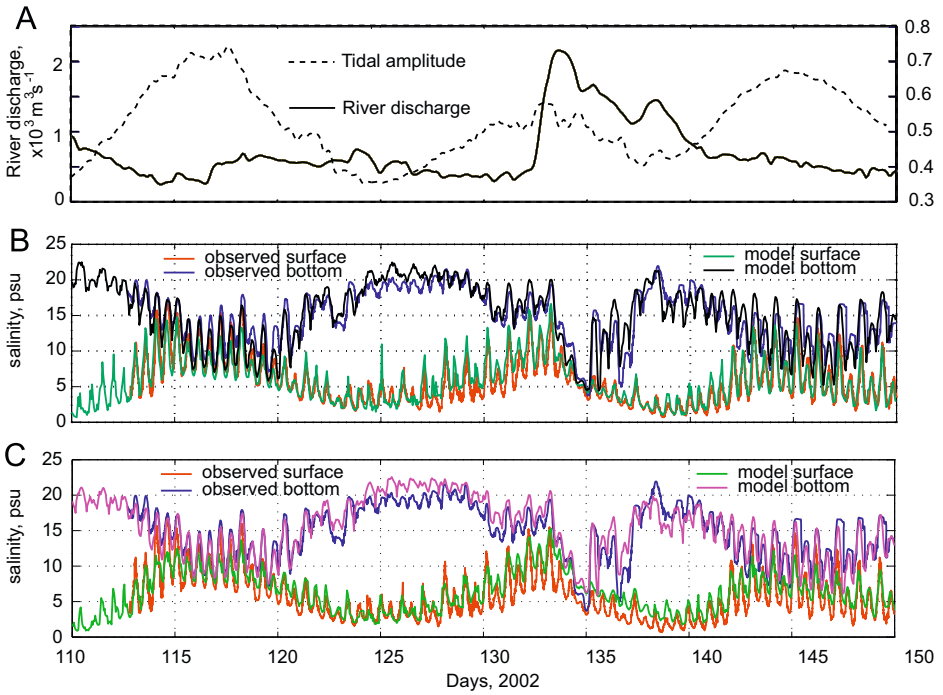

Fig. 4. Estuarine response to river discharge and tidal forcings. (A) Tidal amplitude (dashed line) and river discharge (solid line). Comparison of measured to modeled time series of salinity at site N3 from (B) a single grid using a derived salinity boundary condition (Warner et al., 2005a) to (C) composed grid formulation described in this article.

et al. (2005a). Namely, these are a surface boundary condition of zero stress (no wind) and bottom stress based on a logarithmic velocity profile with a roughness length, z_0=0.002 m. The northern momentum boundary condition imposes the observed river discharge scaled to include lateral inflows. The southern boundary is driven by observed free surface displacement using a reduced-physics barotropic pressure gradient condition. Because of the location of the southern boundary, this water level time series is an average of observations from the Battery and Sandy Hook. Radiation boundary conditions were prescribed for the free surface and baroclinic (three dimensional) momentum.

Additional boundary conditions are also required for the western and eastern edges. At these boundaries similar reduced-physics tidal conditions were imposed. The tide at the Kill Van Kull was the same amplitude as imposed at the southern boundary, but phased to allow tidal propagation into that boundary. At the eastern end, where the domain meets Long Island Sound, the observed water level from Kings Point (Fig. 3) was applied. The tides at the western end of Long Island Sound have an increased amplitude and phase delayed compared to those in New York Harbor. The salinity at the western end was nudged to 28, to 26 at the eastern end, and to 28 at the southern end based on climatology at those locations. Simulation results in the Hudson River were not sensitive to these values.

Parameterizations for subgrid scale mixing of mass and momentum are determined using the Generic Length Scale turbulence closure method (GLS; Umlauf and Burchard, 2003) as implemented by Warner et al. (2005b) with parameters equated to the k–ε formulation. There were no surface tracer fluxes and temperature was held constant at 10 °C. The model was initiated from rest with a stratified salinity field along the lower 50 km of the estuary. The initial bottom salinity values range from 28 at the mouth to 0 at river km 50, with stratification ranging from 10 at the mouth to 0 at the limit of salt intrusion. These values simulate a typical salt intrusion during the simulation period. Hydrodynamic conditions of the estuary were simulated for 50 days; however, the first 10 days provide dynamic adjustment of the density field from initial conditions and are not used in the analysis, consistent with previous findings.

3.2. *Realistic simulations—salinity and dye dispersion processes*

As a test of the composite grid system, first we performed an experiment to model the salt dynamics from 23 April to 5 June 2002 (year days 113–156). This time period is coincident with the observations of Lerczak et al. (2006) and the previous numerical investigation by Warner et al. (2005a). Time series of water level and currents from the composed grid solution at site N3 near river km 23 were compared to and found to be consistent with the observations and the previous numerical simulations. A similar comparison for the time series of salinity is shown in Fig. 4. The top panel (Fig. 4A) shows the tidal amplitude (dashed line) spring/neap variability for the 40 day time period. Spring tides are centered on days 117, 131, and 145, with neap tides centered between these dates. The freshwater inflow was relatively constant around 500 $m^3 s^{-1}$ until a large freshet event that started near day 132 reaching over 2000 $m^3 s^{-1}$. The salinity response to these forcing conditions is shown in panels B and C. During spring tides the increased mixing reduces the stratification. Stratification increases during the neap tides and is almost completely eliminated at the onset of the freshet. Additional details are described in Warner et al. (2005a). Fig. 4B is repeated here from that previous investigation (their Fig. 6). Fig. 4C displays the results from this article using the composite grid approach. Results from the composite grid method are consistent with results from the previous method with a similar skill as computed in Warner et al. (2005a).

It is noteworthy that the composite grid model did not have any tuning of its salinity boundary condition, and it still reproduced the major features of the salinity variations in the domain. Thus the additional model segments in New York Harbor and the East River actually simulated the salinity variations that were empirically tuned to match the data in the Warner et al. (2005a) modeling effort.

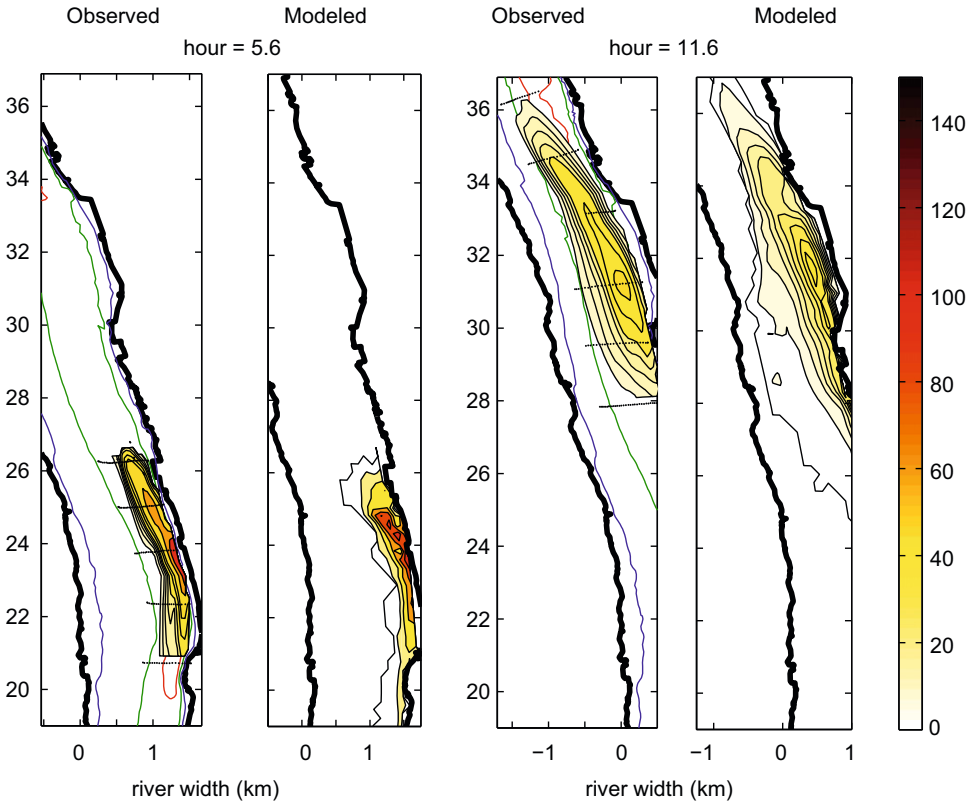

Fig. 5. Plan view comparison of observed to modeled dye release. Left panels at hour 5.6. Right panels at end of flood at hour 11.6. Concentration units of 10^{-8} kg/m^3.

As an additional experiment to determine that the composite grid model was correctly simulating the mixing and transport dynamics in the estuary, a dye release as described by Geyer et al. (2008) was simulated. Four patches of passive tracer were released in the model at different locations and times to coincide with the actual field releases. Both horizontal and vertical spreading of the dye was well represented by the model. Comparisons are shown for the first dye release, which occurred during a neap tide, with the injection near the end of ebb. Fig. 5 compares the vertically averaged dye concentrations observed to that of the model at two instances in time. The model can be seen to correctly predict the along-channel spreading of the dye. At hour 5.6 the model has a slightly more northern displacement of the patch, which could be attributed to the initial location of dye in the model not exactly coinciding with the field study. At hour 11.6 the dye center of mass is nearly coincident with that observed showing accurate simulation of the advection but with a slightly lower level of concentration.

Fig. 6 compares the along-channel vertical structure of the observed dye to that of the model, again for the first neap-tide release. In both observations and the model, the dye is confined to the bottom boundary layer, due to suppression of mixing in the pycnocline. The vertical distribution of dye is consistent between the model and observations. By hour 11.3 (Fig. 6, bottom), the dye has advected farther northward while still being confined in the bottom boundary layer. These comparisons are not comprehensive, but they provide a measure of confidence in the ability of the model to simulate dispersion processes in the estuary.

3.3. *Numerical tracer experiments to determine residence time*

The composite grid approach is particularly useful for quantifying the exchange between the estuary and New York Harbor, which is an essential process affecting the residence time of tracers in the estuary. Actual dye releases in an estuary typically cannot effectively quantify residence time, because the tracer is diluted below the threshold detection level before the dye has spread to the full dimensions of the estuary. Moreover, the field study was influenced by many physical processes in addition to the tides such as subtidal storm oscillations, variability of the freshwater discharges, tides, etc. To isolate the effects of the main tidal processes, we performed an idealized study to investigate the residence time of a tracer. The tracer was released at different vertical locations in the water column and at different phases of the spring/neap cycle. Boundary conditions were the same as described for the realistic simulation except for the following. The model was forced with a steady river discharge of 500 m^3/s (representative of moderate flow conditions) and with only a spring-neap cycle of tidal range. The tide was constructed using the M2 and S2 tidal phase and amplitudes as shown in Table 1.

To investigate the spatial and temporal variability of residence time in the estuary, we released a passive tracer at twelve locations in the estuary: six along the bottom and six near the surface. The locations were evenly spaced along the length of the main channel at 12, 24, 36, 48, 60, and 72 km (as shown in Fig. 3, inset map). Dye was released at each location simultaneously during a neap tide, and then another set of releases was performed during the following spring tide. This resulted in 24 dye releases that were passive and non-interactive, i.e., not influencing the density or each other. For the next two Sections (3.3.1 and 3.3.2), we will focus on results from the km 24 release location and describe the variability of the surface vs. bottom and neap vs. spring release. Then (Section 3.4), all 24 releases will be used to define the spatial structure of dispersion in the estuary.

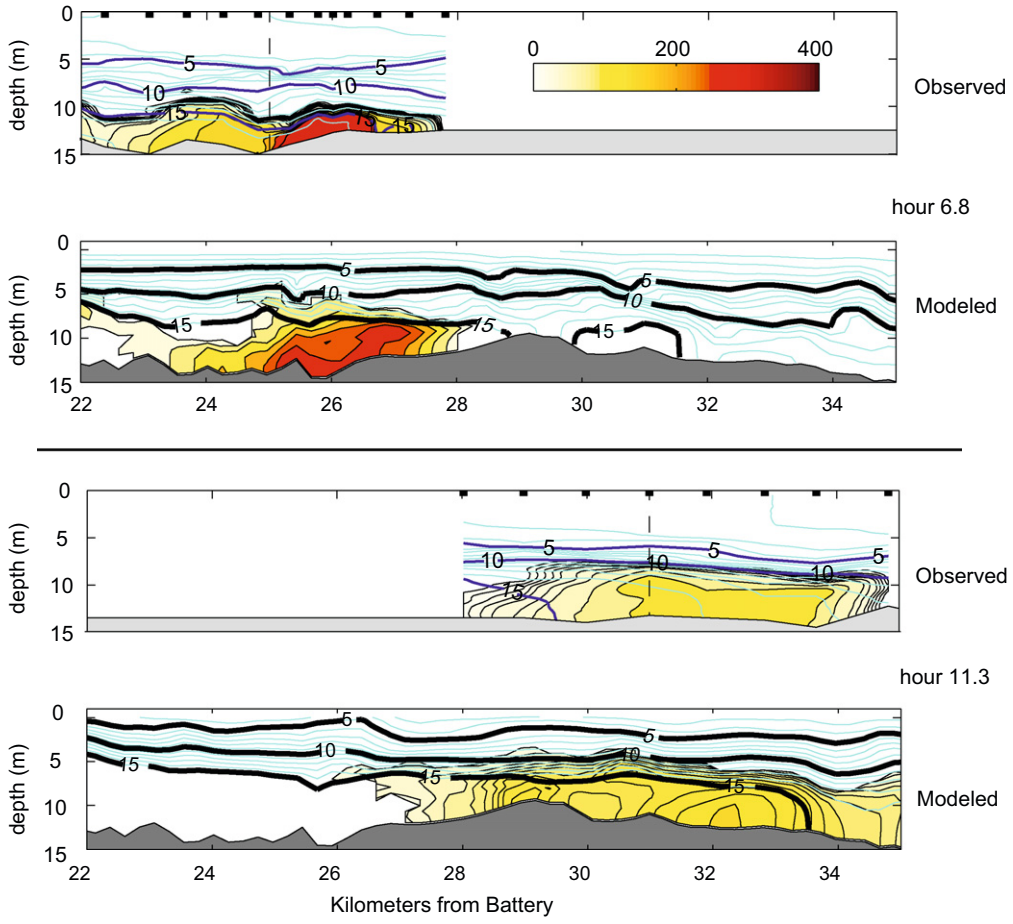

Fig. 6. Along-channel vertical transects of observed and modeled dye.

Table 1
Boundary amplitude and phases for the idealized spring/neap experiments.

Boundary location	M2		S2	
	Amp (m)	Phase (deg)	Amp (m)	Phase (deg)
Southern end (Raritan Bay)	0.66	18.53	0.25	45.03
Western end (Kill Van Kull)	0.66	18.53	0.25	45.03
Eastern end (East River)	1.15	115.2	0.40	142.43

3.3.1. *Idealized neap tide release at km 24*

Fig. 7 shows depth-averaged results from the neap tide release at three instances in time after release: end of first ebb ($t=6$ h), end of first flood ($t=12$ h), and after 3 days near the end of flood tide. The top panels are for the near-bottom release and the lower panels are for the near-surface release. In each case, the dye was released at early ebb. After the end of the first ebb (Fig. 7, left column), the mean current has stretched the dye approximately 10 km along the channel. More of the dye has remained closer to the release location for the near-bottom release because the bottom currents are weaker during ebb, and more of the dye has advected southward in the near-surface waters than in the bottom layer because the surface currents are stronger. By the end of the first flood (Fig. 7, middle column), the center of mass of the near-bottom release has advected substantially farther up-estuary due to the stronger near-bottom current resulting from the estuarine circulation. The near-surface currents are weaker during the flood, and so the center of mass does not advect as far into the estuary for the surface release. This process continues for several tidal cycles, with the near-bottom release being advected further into the estuary due to the estuarine circulation, and the near-surface release being advected further out of the estuary due to the stronger ebb surface currents. This creates a significant difference in the transport pathway of the tracer, dependent on its initial release location. By the end of 3 days (Fig. 7, right column), the near-bottom release still has a large quantity of the dye heading landward due to the estuarine circulation, while a majority of the dye from the surface release has exited the estuarine part entered into the harbor and even exited the harbor.

These processes can be explained further by observing the vertical variation of the same neap tide near-surface and near-bottom dye releases along the length of the salt intrusion in the thalweg. Fig. 8 shows the tracer concentrations at the same instances as in Fig. 7: end of first ebb at $t=6$ h, end of first flood at $t=12$ h, and at $t=3$ days at end of flood. At the end of the first ebb (Fig. 8, top row), the near-bottom release dye (left side) initially mixes vertically but only up to the pycnocline, which is high in the water column, probably overestimated as was noted earlier. The stratification during neap tides inhibits the vertical mixing of the dye over the entire depth. The tracer patch is slightly tilted in the seaward direction due to the shear of the ebb current. For the near-surface release (right side) the tracer mass remains in the surface layer and is advected seaward rapidly. At the end of the first flood (Fig. 8, middle row) the bottom release (left side) is now more uniformly dispersed and the center of mass has advected landward to river km 30. The near-surface release (right side) has been strained and now stretches along a 15 km section of the estuary, with most of the dye still in the upper half of the water column. The center of mass has moved towards the harbor due to the mean seaward transport in the surface layer. After 3 days

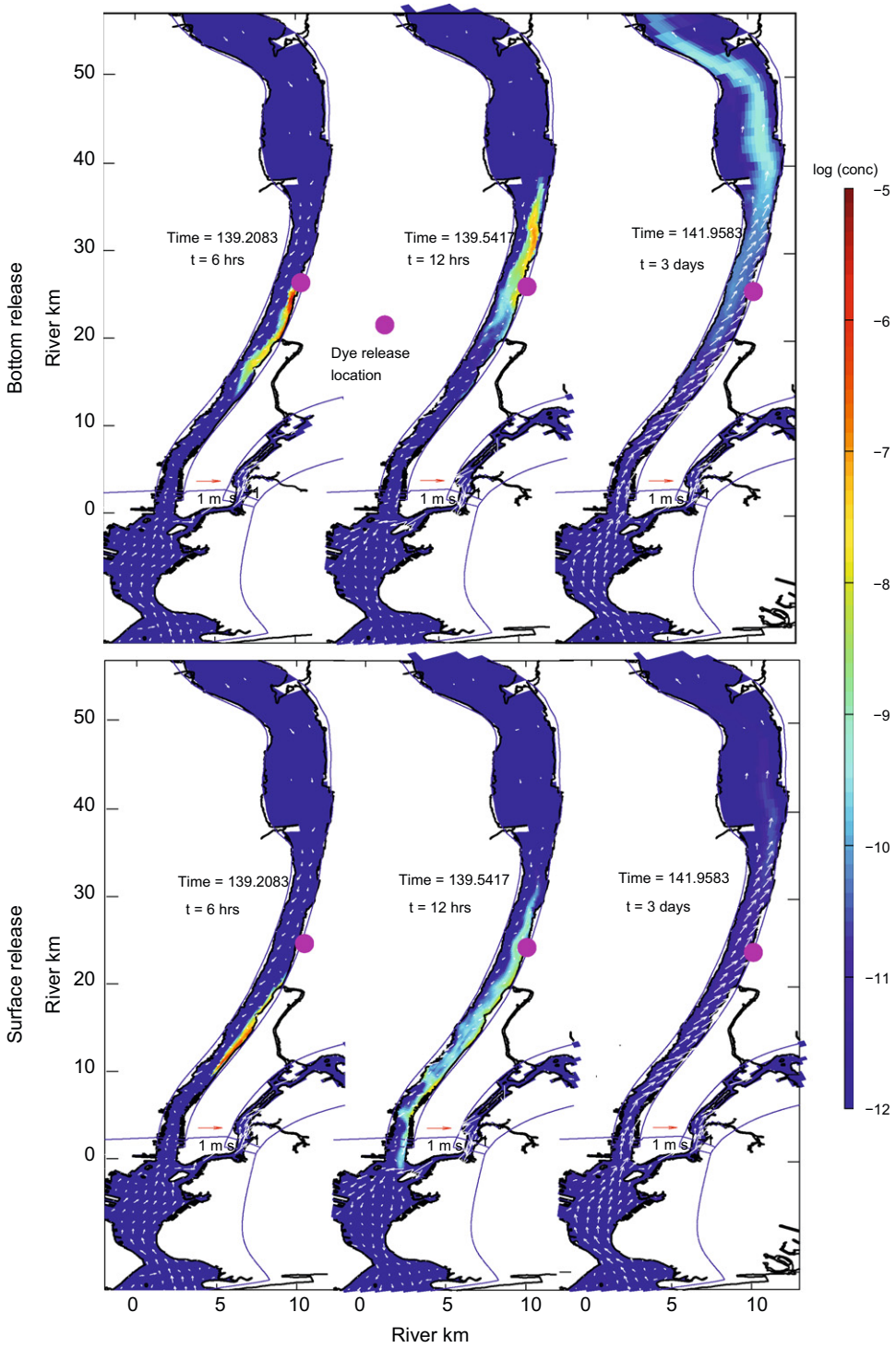

Fig. 7. Plan view of depth averaged dye concentrations for NEAP TIDE release at km 24 (Left column, end of first ebb; middle column, end of first flood; right column, after 3 days near end of flood tide) (same times as in Fig. 8). Top panels = near-bottom release, bottom panels = near-surface release.

(Fig. 8, bottom row), the tracer patches have diluted by several orders of magnitude relative to the initial release. However the model can still account for location of the tracer. The center of mass for the near-bottom release (left side) continues to advect landward due to the residual estuarine circulation. During each tidal cycle, tracer mass is sheared from the main location and mixes along the isohalines into the surface layer. The tracer then exits the estuary through this surface layer. The tracer mass for the near-surface release (right side) has predominately exited the estuary, and its concentration is an order of magnitude lower than the bottom release. The dye that remains has been mixed along isohalines and is now in the bottom boundary layer, advecting landward in a similar fashion as the near-bottom release.

3.3.2. *Spring tide release at km 24*

As expected, there was a dramatic difference between the spreading of tracer during the spring tide as compared to the neap tide. The near-surface and bottom spring tide dye was also released at slack before ebb (at river km 24 again, Fig. 9). By the end of the first

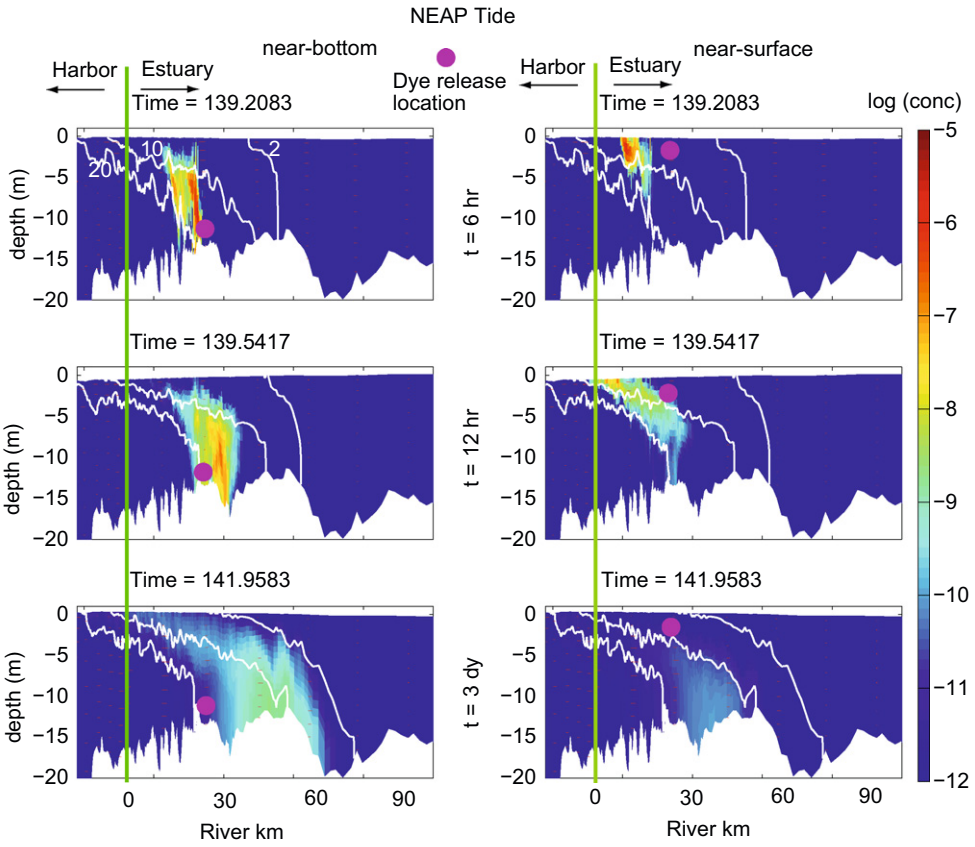

Fig. 8. Profile view of laterally averaged dye concentrations for NEAP TIDE release at km 24. (A) end of first ebb; (B) end of first flood; (C) after 3 days near end of flood tide (same times as in Fig. 7). Left panels = near-bottom release, right panels = near-surface release. Salinity contours of 2, 10, and 20 are shown as white lines.

ebb at $t = 6$ h, the dye is stretched along the thalweg of the estuary for a distance of approximately 10 km. This distance is about the same for both the surface and bottom releases, and the center of mass for both releases is approximately the same at ~10 km south of the release location. By the end of the first flood at $t = 12$ h (Fig. 9, middle column), it is clear that the centers of mass for both releases are approximately consistent in the along-channel location. The tracer now stretches approximately 20 km in length with the center of mass now advected near the initial release location. After 3 days, the near-bottom and surface releases have nearly the same distributions (Fig. 9, right column). The tracer has spread along the lower ~30 km of the estuary and into the harbor.

The reason that the near-surface and bottom dye releases are similar during spring tides becomes apparent by observing the vertical structure of the dye (Fig. 10). During spring tides there is stronger tidal mixing and the isohalines are nearly vertical. The tracer mixes vertically all the way to the surface within one tidal cycle. This process is also confirmed by the observations as noted by Geyer et al. (2008). After 6 h, the near-bottom and surface releases (Fig. 10, top row) show a vertically mixed tracer with very little vertical shearing of the dye. By the end of the first flood at 12 h (Fig. 10, middle row) the dye is vertically well mixed with a slight indication of near-surface shear. However, there is minimal difference when comparing the near-surface release to the near-bottom release. After 3 days (Fig. 10, bottom row) the tracer for both the surface and bottom releases is essentially indistinguishable.

3.4. Quantification of residence time

To provide a quantitative assessment of the residence time of these releases, the mass of each tracer was summed at each time step in the estuarine section of the model. This total mass was then plotted vs. time (Fig. 11). The residence time is then the integrated normalized concentration for each release (for example, Yuan et al., 2007, Eq. 12 or Delhez et al., 2004, Eq. 4). Based on this definition, the residence time depends on the location and the time within the spring-neap cycle that it is released. Although it would be impossible to estimate residence time this way in a real estuary due to dilution and sampling limitations, it is straightforward to introduce numerical tracers within the model at different times and places and to quantify their rate of decrease with time.

The residence time computations are shown in Fig. 11 for the four releases described in the last section. The top panel shows a time series of water level to identify the spring/neap tidal phasing. The bottom panel shows the estimate of residence time for each release. During the neap-tide near-bottom release (blue line), very little dye leaves the estuary for the first several days because the majority of the dye is maintained in the bottom boundary layer and advected landward due to the estuarine circulation. Most of the tracer remains in the estuary until the next neap tide, and this release has a computed residence time of 15 days. For the near-surface neap tide release (red line), the tracer does not mix vertically due to the strong stratification and the majority of the dye is transported seaward in the surface currents and advected out of the estuary. The residence time of the near-surface neap release is 5 days. For the spring tide releases (surface and bottom), the water column is mostly unstratified, and the dye quickly mixes vertically for both the surface and bottom release. This results in almost identical residence times of approximately 7 days for each (black and magenta lines).

We computed the residence time in a similar manner for all the releases in the estuary (km 12, 24, 36, 48, and 60)

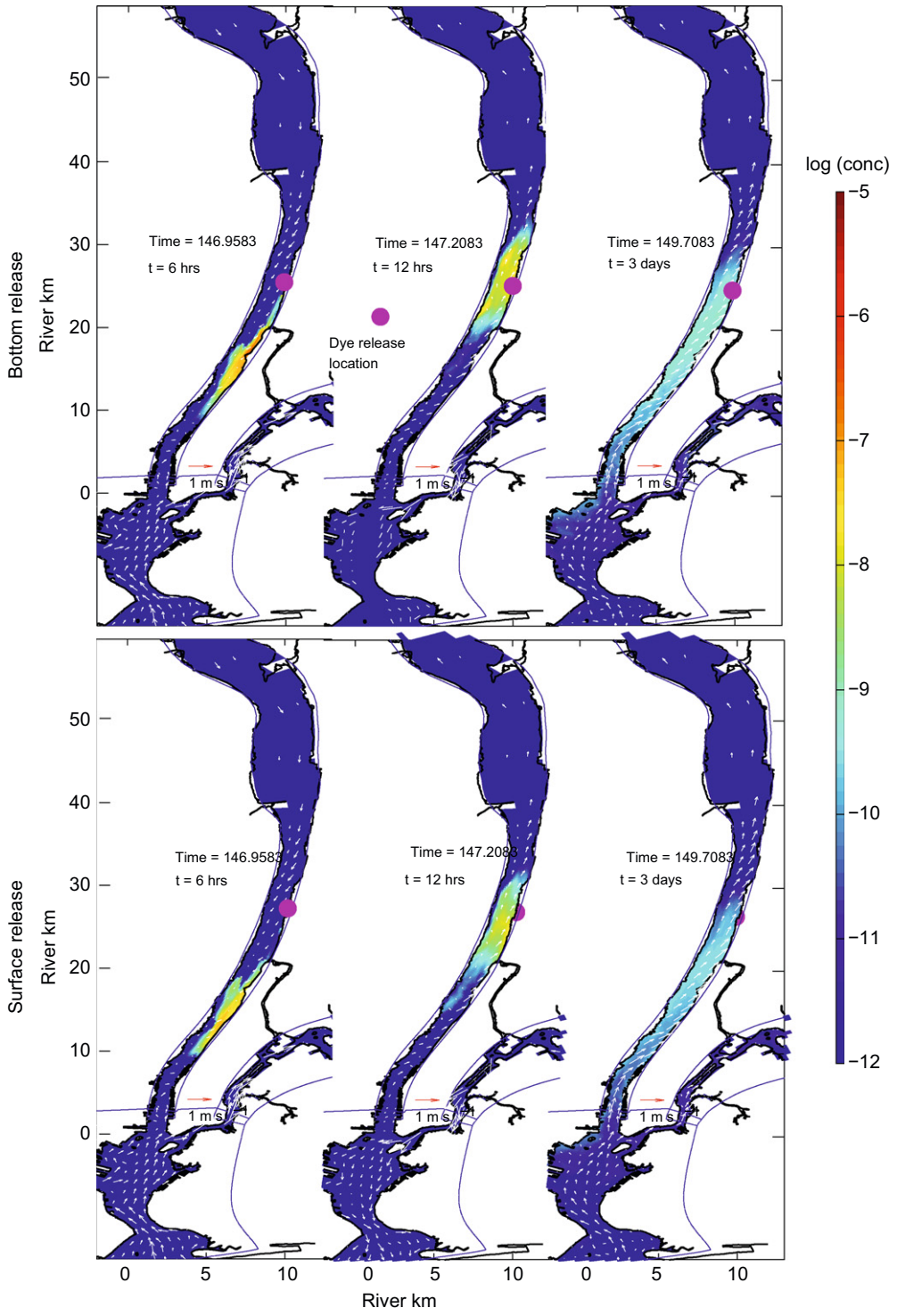

Fig. 9. Plan view of depth averaged dye concentrations for spring tide release at km 24. (Left column, end of first ebb; middle column, end of first flood; right column, after 3 days near end of flood tide) (same times as in Fig. 10). Top panels = near-bottom release, bottom panels = near-surface release.

near-bottom and near-surface for both neap and spring tides. The residence times estimated from different sites in the estuary show considerable variability. During neap tides (Fig. 12, top) the residence times of the near-surface water is very short (order 2 days) due to the close proximity to the mouth. Moving landward the residence time increases almost linearly to about 20 days at km 70. This demonstrates a seaward advective process, consistent with the estuarine circulation. For the near-bottom residence time, there is a mid-estuary maximum of 18 days around 30–40 km. There is a local minimum of 12 days around 50 km, beyond which the residence time monotonically increases. This complex pattern of residence time is due to the combination of the estuarine circulation, tides, and freshwater advection, modulated by the spring-neap cycle. The residence-time minimum at 50 km is the convergence point for net bottom-water advection: water parcels both landward and seaward have longer trajectories and thus longer residence times. The landward water is advected by the net riverine outflow, and the seaward

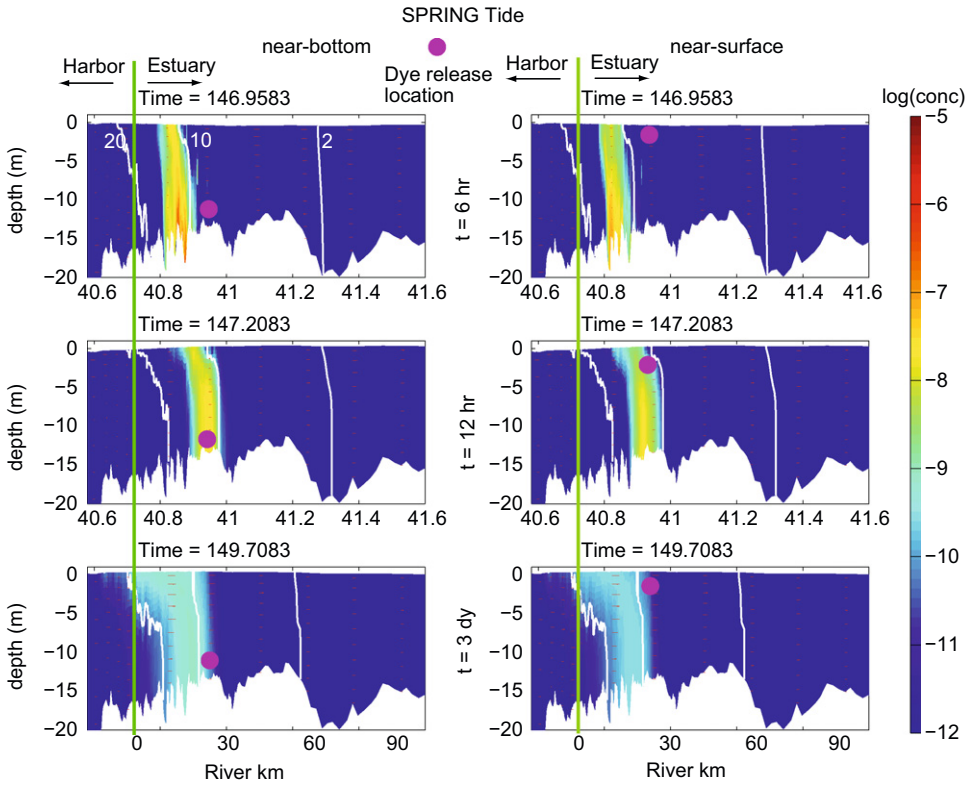

Fig. 10. Profile view of laterally averaged dye concentrations for spring tide release at km 24. (A) end of first ebb; (B) end of first flood; (C) after 3 days near end of flood tide (same times as in Fig. 9). Left panels=near-bottom release, right panels=near-surface release. Salinity contours of 2, 10, and 20 are shown as white lines.

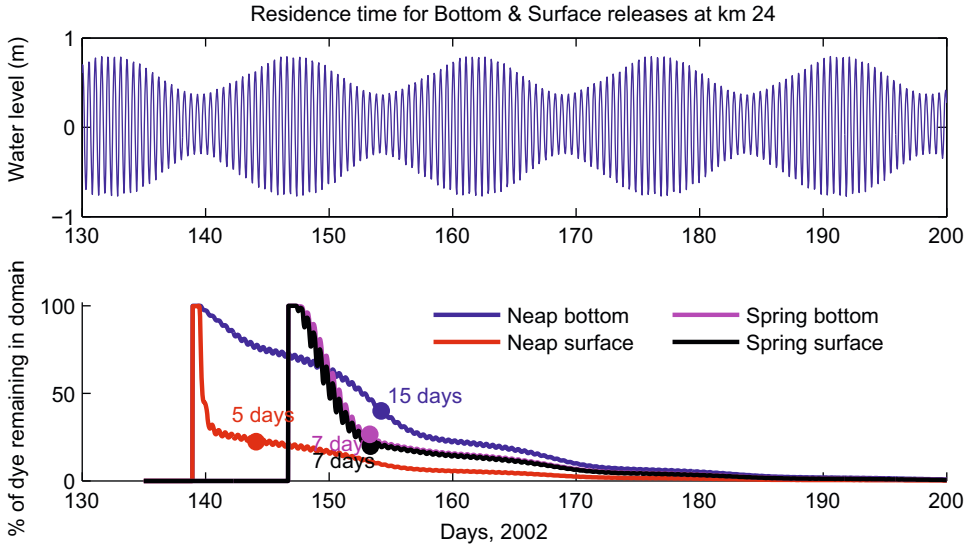

Fig. 11. Residence time as a function of percent of dye remaining for each tracer release at km 24. Top panel is a time series of water level to identify spring/neap cycle. Bottom panel is time series of percent of dye remaining in the estuarine portion of the domain. The time integral of percent dye remaining provides a computation of residence time with values shown for these releases.

water is advected by the estuarine circulation. The decrease in residence time within one tidal excursion of the mouth is readily explained by tidal dispersion, i.e., dye is advected out of the mouth during the ebb, and exchange with harbor water leads to net export. The lower near-bottom residence times between 12 and 25 km are harder to explain, because the influence of tidal dispersion would not be expected to occur at a location two tidal excursions from the mouth. However, these lower residence times indicate the influence of vertical exchange, which transports some of the dye from the lower layer into the upper water column (cf. Fig. 8), whereupon it is advected out of the estuary. Note that most of these residence times are longer than 7 days, so the estuary experiences a neap-to-spring transition before the water can be carried out. Although vertical mixing is not very strong during neap tides, the residence times exceeding 7 days include the integrated influence of both neap and spring-tide conditions.

During spring tides it was previously demonstrated that the dye mixes vertically within ~1 day, and so there is little difference

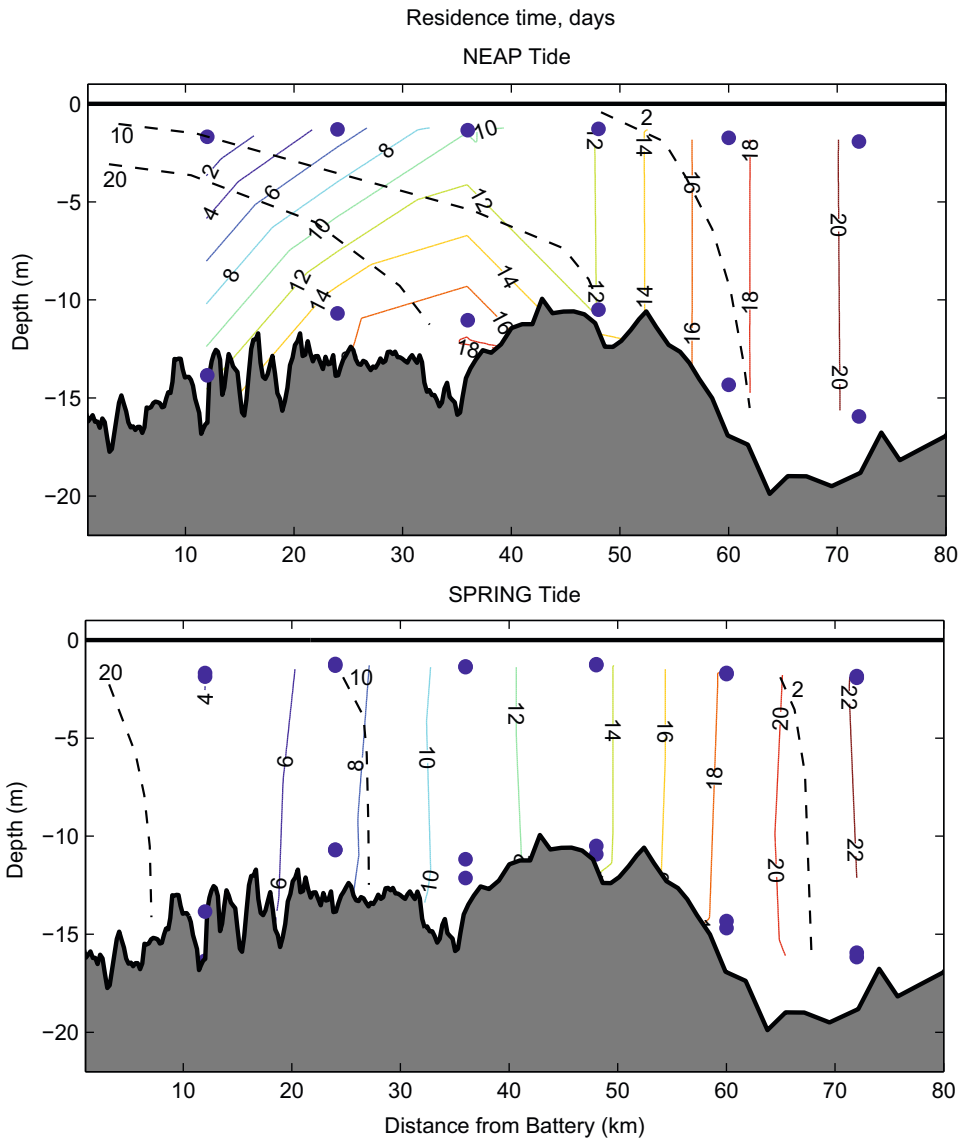

Fig. 12. Contours of residence time (solid lines) for all surface and bottom dye releases. Top panel is for neap tide release showing a mid-estuary near-bottom maximum. Bottom panel is for spring tide releases revealing residence time as primarily a function of longitudinal location. Salinity contours (dashed lines) for 20, 10, and 2. Blue dots are tracer release locations. (For interpretation of the references to color in this figure legend, the reader is referred to the web version of this article.)

between the bottom and surface releases. This is apparent in the spatial variability of the residence time (Fig. 12, lower panel). During spring tides, there is much less difference in residence time between near-surface and near-bottom waters, and the residence times show a monotonic increase with distance from the mouth. The residence time ranges from near 8 days at the mid-estuary salt intrusion to approximately 20 near the limit of salt intrusion. This distribution is more consistent with horizontal dispersion process than the advective process occurring during the neaps. Within one tidal excursion of the mouth, tidal exchange (as described above) result in short residence times, but vertical and lateral shear dispersion become more important between 15 and 40 km from the mouth. Although the estuary is relatively well mixed during the springs, there is some tendency for the surface waters to be carried seaward relative to the bottom waters (Fig. 10), leading to net horizontal dispersion (Fischer et al., 1979). Likewise lateral shears lead to net dispersion, as shown by the laterally skewed distributions in Fig. 9. Landward of 40 km, the residence times are long enough that the transport is significantly affected by the return to neap conditions, with the associated advective transport. The spring residence times in this part of the estuary are longer than they are during neaps, because the advective transport is impeded by the strong mixing during springs.

The residence time estimates can be contrasted to the advective timescale of the river outflow without tides or estuarine circulation. The mean outflow during this simulation resulted in a vertically averaged seaward velocity of about 3 km/day. This rate is comparable to the spring tide residence time (i.e., at 60 km the residence time would be 60 km/3 km/day = 20 days, comparable to Fig. 12, bottom).

The along-estuary distribution of residence times is not linear due to the additional contribution of tidal dispersion. Using a simple model for residence time assuming that both advection and dispersion contribute to the flux of dye, an expression for the residence time is given by

$$T_{res} = \frac{X}{\overline{u} + \frac{K}{X}} \tag{1}$$

where X is the distance along the estuary, $\overline{u}$ is the mean outflow velocity, and K is the effective dispersion rate. Using the along-estuary residence time estimates from the spring-tide release

(Fig. 12, bottom), Eq. 1 can be used to estimate K. Its value is found to be close to $500\,m^2\,s^{-1}$ near the mouth, decreasing to $100–200\,m^2\,s^{-1}$ between 30 and 50 km. These values are consistent with field estimates of tidal dispersion (Geyer et al., 2008) and with the expectation that the dispersion rate increases near the mouth due to "non-local" exchange processes (Stommel and Farmer, 1952; Dronkers and van de Kreeke, 1986; Banas and Hickey, 2005). Farther landward, the estimate becomes negative, indicating that the assumptions leading to Eq. 1 are invalid in this part of the domain (e.g., the neglect of estuarine circulation processes in regions of long residence time, in which the following neap tide plays a major role).

4. Summary and conclusions

We have demonstrated the methodology to create a multi-grid framework that allows an unlimited number of grids to be seamlessly connected to yield a composed grid structure. Time integration of grid points near the mesh interface is performed using data fields from the adjacent mesh. We successfully applied the composite grid method to first an idealized application to demonstrate the complete accuracy of the method, and then to a realistic estuarine setting to estimate residence time of a neutrally buoyant passive tracer. This application indicates that the spring-neap cycle and vertical location of the tracer release has a large and complex influence on residence time. During neap tides there is a mid-estuary near-bottom maximum in residence time created due to a combination of the estuarine circulation and the tidal advection in proximity to the estuary mouth. During spring tides the water column is well mixed and the residence time was more associated with the along-channel location of the release and did not exhibit strong vertical variability. The composite grid approach would be useful in a variety of applications in coastal and estuarine environments with complex morphologies.

Acknowledgments

W.R. Geyer was supported by the Hudson River Foundation Grant 002/07A, H.G. Arango by the Office of Naval Research, and John Warner was supported by the USGS Community Sediment Modeling Project. We greatly acknowledge the use of the bathymetry data obtained from Roger Flood of SUNY Stony Brook and John Ladd from the Hudson River National Estuarine Research Reserve, Hudson River Estuary Program, New York State Department of Environmental Conservation.

References

Abood, K.A., 1974. Circulation in the Hudson estuary. In: Roels, O.A. (Ed.), Hudson River Colloquium, 250. Annals of the New York Academy of Sciences, pp. 38–111.

Aikman, F.A., Lanerolle, L.W.J., 2004. Report on the National Ocean Service Workshop on Residence/Flushing Times in Bays and Estuaries. NOAA Office of Coast Survey, Silver Spring, MD. 〈http://www.nauticalcharts.noaa.gov/csdl/residencetime.html〉.

Arakawa, A., Lamb, V.R., 1977. Computational design of the basic dynamical process of the UCLA general circulation model. Methods in Computational Physics 17, 173–265.

Banas, N.S., Hickey, B.M., 2005. Mapping exchange and residence time in Willapa Bay, Washington, a branching, macrotidal estuary. Journal of Geophysical Research 110, C11011, doi:10.1029/2005JC002950.

Barad, M.F., Colella, P., Schladow, S.G., 2009. An adaptive cut-cell method for environmental fluid mechanics. International Journal for Numerical Methods in Fluids 60, 473–514, doi:10.1002/fld.1893.

Bolin, B., Rodhe, H., 1973. A note on the concepts of age distribution and residence time in natural reservoirs. Tellus 25, 58–62.

Bowen, M.M., Geyer, W.R., 2003. Salt transport and the time dependent salt balance of a partially stratified estuary. Journal of Geophysical Research, Oceans 108 (C5), 3158, doi:10.1029/2001JC001231.

Debreu, L., Blayo, E., 2008. Two-way embedding algorithms: a review. Ocean Dynamics 58, 429–440 Special issue on multi-scale modelling: nested grid and unstructured mesh approaches.

Deleersnijder, E., Campin, J.-M., Delhez, E.J.M., 2001. The concept of age in marine modelling: I. Theory and preliminary model results. Journal of Marine Systems 28, 229–267.

Deleersnijder, E., Lermusiaux, P., 2008. Multi-scale modeling: nested-grid and unstructured-mesh approaches. Ocean Dynamics 58, 335–336.

Delhez, E.J.M., Heemink, A.W., Deleersnijder, E., 2004. Residence time in a semi-enclosed domain from the solution of an adjoint problem. Estuarine, Coastal and Shelf Science 61, 691–702.

Dietrich, D.E., Tseng, Y.H., Medina, R., Piacsek, S.A., Liste, M., Olabarrieta, M., Bowman, M.J., Mehra, A., 2008. Mediterranean overflow water (MOW) simulation using a coupled multiple-grid Mediterranean Sea/North Atlantic Ocean model. Journal of Geophysical Research, Oceans 113, C07027, doi:10.1029/2006JC003914.

Dronkers, J., van de Kreeke, J., 1986. Experimental determination of salt intrusion mechanisms in the Volkerak estuary. Netherlands Journal of Sea Research 20, 1–19.

Eby, M., Holloway, G., 1994. Grid transformation for incorporating the Arctic in a global ocean model. Climate Dynamics 10, 241–247.

Fischer, H.B., List, E.J., Kho, R.C.Y., Imberger, J., Brooks, N.H., 1979. Mixing in Inland and Coastal Waters. Academic Press, New York 483pp.

Geyer, W.R., Cannon, G.A., 1982. Sill processes related to deep water renewal in a fjord. Journal of Geophysical Research 87, 7985–7996.

Geyer, W.R., Chant, R., Houghton, R., 2008. Tidal and spring-neap variations in horizontal dispersion in a partially mixed estuary. Journal of Geophysical Research, Oceans 113, C07023, doi:10.1029/2007/JC004644.

Geyer, W.R., Trowbridge, J.H., Bowen, M.M., 2000. The dynamics of a partially mixed estuary. Journal of Physical Oceanography 30, 2035–2048.

Gourgue, O., Deleersnijder, E., White, L., 2007. Toward a generic method for studying water renewal, with application to the epilimnion of Lake Tanganyika. Estuarine, Coastal and Shelf Science 74, 628–640.

Haidvogel, D.B., Arango, H.G., Budgell, W.P., Cornuelle, B.D., Curchitser, E., Di Lorenzo, E., Fennel, K., Geyer, W.R., Hermann, A.J., Lanerolle, L., Levin, J., McWilliams, J.C., Miller, A.J., Moore, A.M., Powell, T.M., Shchepetkin, A.F., Sherwood, C.R., Signell, R.P., Warner, J.C., Wilkin, J., 2008. Regional ocean forecasting in terrain-following coordinates: model formulation and skill assessment. Journal of Computational Physics 227, 3595–3624.

Lerczak, J.A., Geyer, W.R., Chant, R.J., 2006. Mechanisms driving the time-dependent salt flux in a partially stratified estuary. Journal of Physical Oceanography 36, 2296–2311.

Liu, W.C., Chen, W.B., Kuo, J.T., Wu, C., 2008. Numerical determination of residence time and age in a partially mixed estuary using three-dimensional hydrodynamic model. Continental Shelf Research 28, 1068–1088.

Monsen, N.E., Cloern, J.E., Lucas, L., Monismith, S., 2002. A comment on the use of flushing time, residence time, and age as transport time scales. Limnology and Oceanography 47, 1545–1553.

Penven, P., Debreu, L., Marchesiello, P., McWilliams, J.C., 2006. Evaluation and application of the ROMS 1-way embedding procedure to the central California upwelling system. Ocean Modelling 12 (1–2), 157–187.

Shchepetkin, A.F., McWilliams, J.C., 2005. The regional ocean modeling system: a split-explicit, free-surface, topography-following coordinates ocean model. Ocean Modelling 9, 347–404.

Stommel, H., Farmer, H.G., 1952. On the nature of estuarine circulation. Woods Hole Oceanographic Institute, Technical Report No. 52–88, 131pp.

Takeoka, H., 1984. Fundamental concepts of exchange and transport time scales in a coastal sea. Continental Shelf Research 3, 311–326.

Umlauf, L., Burchard, H., 2003. A generic length-scale equation for geophysical turbulence models. Journal of Marine Research 61, 235–265.

Wolanski, E., 2007. Estuarine Ecohydrology. Elsevier, Amsterdam, The Netherlands 157pp.

Warner, J.C., Geyer, W.R., Lerczak, J.A., 2005a. Numerical modeling of an estuary: a comprehensive skill assessment. Journal of Geophysical Research, Oceans 110, C05001, doi:10.1029/2004JC002691.

Warner, J.C., Sherwood, C.R., Arango, H.G., Signell, R.P., 2005b. Performance of four turbulence closure models implemented using a generic length scale method. Ocean Modelling 8, 81–113.

Yuan, D., Lin, B., Falconer, R.A., 2007. A modeling study of residence time in a macro-tidal estuary. Estuarine, Coastal, and Shelf Science 71, 401–411.

Zhang, W.G., Wilkin, J.L., Schofield, O.M.E., 2010. Simulation of water age and residence time in New York Bight. Journal of Physical Oceanography, 10.1175/2009JPO4249.1.

Zimmerman, J.T.F., 1976. Mixing and flushing of tidal embayments in the Western Dutch Wadden Sea, part II: analysis of mixing processes. Netherlands Journal of Sea Research 10, 397–439.

Zimmerman, J.T.F., 1986. The tidal whirlpool: a review of horizontal dispersion by tidal and residual currents. Netherlands Journal of Sea Research 20, 133–154.